JOURNAL OF AIRCRAFT
Vol. 33, No. 1, January–February 1996

Experiments and Analysis for a Gust Generator in a Wind Tunnel

D. M. Tang,* Paul G. A. Cizmas,† and E. H. Dowell‡
Duke University, Durham, North Carolina 27708-0300

An experimental investigation was made of the gust field generated by a rotating slotted cylinder installed in the Duke University low-speed, closed-circuit wind tunnel. The system has a very simple configuration with low cost and can produce a controllable single or multiple harmonic gust wave in the lateral and longitudinal directions. It requires minimal power and torque input. A simplified theoretical aerodynamic model and a design estimation of the lateral and longitudinal gust flowfield is also proposed in this article. The design estimate is based on a two-dimensional dynamic lift coefficient that is given by the theoretical and experimental results. An interfering wake vortex effect is the major disadvantage of this system.

Nomenclature

$C(k)$	=	Theodorsen's function
$\|C_{leq}\|$	=	magnitude of equivalent lift coefficient for rotating slotted cylinder/airfoil
c	=	airfoil chord
d	=	cylinder diameter
dL_a	=	airfoil lift force per span length
dL_{rsc}	=	rotating slotted cylinder lift force per span length
e, $\bar{e}$	=	gap between the o.d. of the rotating slotted cylinder and trailing edge of the airfoil, e/c
H, $\bar{H}$	=	vertical position from tunnel bottom, H/H_w
H_w	=	height of the tunnel test section
k	=	reduced frequency, $\omega c/2u$
L, $\bar{L}$	=	longitudinal position from cylinder centerline, L/c
R, $\bar{R}$	=	distance between cylinder center and the pressure probe, R/c
u	=	freestream velocity
v_1, v_2	=	induced velocities induced by Γ_1 and Γ_2
X, Y, Z	=	fixed coordinate system, Fig. 1a
y_p, $\bar{y}_p$	=	lateral position from tunnel centerline, y_p/c
y_0, $\bar{y}_0$	=	distance between adjacent cylinders, y_0/c
α_g	=	gust angle of attack, $\Delta w/u$
Γ_1, Γ_2	=	vortex strength for rotating slotted cylinder/airfoils 1 and 2
Δu	=	longitudinal gust velocity
Δw	=	lateral gust velocity
ρ	=	air density
ψ_d	=	dynamic phase difference between adjacent cylinders
ψ_s	=	static (fixed) rotation angle for all cylinders
ω_s	=	cylinder rotation speed
ω_1	=	gust frequency, $2\omega_s$
ω_2	=	gust frequency, $4\omega_s$

I. Introduction

IN recent years, various mechanisms for creating an oscillating flow in a wind tunnel have been developed for the purpose of studying the response of structures to gust excitation. These methods include oscillating biplane vanes mounted on the side walls of the test section entrance,[1] a cascade of oscillating airfoils,[2–4] fixed airfoils with oscillating flaps,[5,6] fixed airfoils with oscillating jet flaps,[7] and airfoils with circulation control.[8] Also, an analytical study of the flowfield in the wake of a cascade of oscillating airfoils and airfoils with oscillating flaps is given in Ref. 9. These conventional gust generators require mechanical complexity to achieve the required sinusoidal lateral and longitudinal gust amplitude over a useful frequency range. Thus, there is a need for a new concept for a gust generator with a high degree of mechanical simplicity, controllability, and reliability. A new flight flutter excitation system invented by Reed[10,11] has been employed successfully in aircraft aeroelastic response investigations. This excitation system has a very simple configuration and can produce hf, high-force aerodynamic excitation with minimal power and torque input.

The principle of the new gust generator is similar to that of two parallel airfoils with circulation control or oscillating jet flaps. The latter needs an air supply source and a more complex airfoil configuration to control the circulation or jet, and thus, the gust magnitude. The former uses the local inflow airstream as an energy source. The new gust generator can induce a controlled gust field in the test section by means of a fixed airfoil with a rotating slotted cylinder (RSC) at its trailing edge. Here the lateral and longitudinal gust intensities are controlled by the RSC. The extremely simple RSC/airfoil system combined with low cost is a major advantage of this gust generator. A gust generator based on the previous flight flutter excitation system was designed by Dynamic Engineering Incorporated and installed in the Duke University low-speed wind tunnel.

An investigation has been made and described in this article of the RSC/airfoil system, including development of an experimental apparatus as well as the associated measurement technique for the gust angle, dynamic lift coefficient of a RSC/airfoil system, and flowfield characteristics. Also, the flowfield around the gust generator device has been numerically simulated using the general purpose finite element program (FIDAP). In the simulation the flow is assumed to be quasisteady, turbulent, incompressible, and two dimensional. The variation of lift as a function of the rotating angle and as a function of the gap between the airfoil and the RSC is calculated. A simplified theoretical aerodynamic model suitable for the design estimation of the lateral and longitudinal gust flowfield is proposed in this article based on the previous theoretical and experimental results.

Received April 20, 1995; revision received Aug. 2, 1995; accepted for publication Aug. 4, 1995.

*Research Associate, Department of Mechanical Engineering and Materials Science.
†Research Assistant, Department of Mechanical Engineering and Materials Science.
‡Professor and Dean, School of Engineering.

Four types of gust flowfields were investigated experimentally including a single harmonic gust, two harmonic components, a continuous linear frequency sweep gust, and a specific designed gust flowfield. The effects of geometrical and kinematic parameters including the distance between the adjacent cylinders, cross-sectional profiles of the RSC, and the dynamic phase difference between adjacent RSC are discussed. A comparison of measured data with a designed gust field was also made. It was found that the simplified theory, although useful for experimental design purposes, needs to be improved. Experimental data and results over a range of parameters provide useful information for improving the present gust generator. The wake vortex effect is the major disadvantage of this RSC system. Finally, while this gust generator was developed with aerospace, and more particularly helicopter, applications in mind, it is believed the device and approach will also prove useful in other applications, e.g., in gust excitation of bridge and building models.

II. Gust Generator System

The gust generator system installed in the Duke University low-speed wind tunnel is a novel device based upon a recently patented concept, the RSC.[10,11] The basic design of the gust generator consists of an aluminum frame, holding a maximum of four vanes, and also a motor drive system. Each vane is a symmetrical airfoil with a 1-in.-diam RSC located at the trailing edge. The vane is simply constructed using a fine-grain wood over an aluminum spar, with a chord length of 4 in., spar length of 20.7 in., and a NACA 0015 airfoil profile. The distance between adjacent vanes is equal to one chord length. The cylinder is made from an aluminum tube with an o.d. of 1 in. and a thickness of one-eighth in. The slot is symmetrical with a 45-deg center angle (base section profile, model A, see Fig. 15). The slot is divided into two spanwise segments, supported by an intermediate ring with a diameter of 1 in. and a width of 0.1 in. The gap between the o.d. of RSC and the trailing edge of the airfoil is one-eighth in. The RSC has two tip bearings that are centrally mounted on the top and bottom plate of a frame. The frame is mounted to a very heavy support table that is attached to the ground. The frame is 6 in. in width and 27.3 in. tall. It is inserted at the test section entrance of the wind tunnel. The top and bottom plate of the frame are aligned with the ceiling and floor of the tunnel test section without being attached to them. The gap between the tunnel and frame is covered by a piece of adhesive tape. The two side plates of the frame are covered by a thin aluminum skin to provide the symmetrical airfoil shape.

Rotation of the cylinders is provided by a dc servomotor. The interface between the motor and cylinders is located on the lower part of the frame through a motor drive system of timing belts and lightweight pulleys. The phase angle between adjacent cylinders, which controls the gust amplitude, is set manually by the relative positioning of the timing belts. In order to obtain a periodic gust angle of attack with two harmonic frequency components (a fundamental frequency component plus a double frequency component) for a given motor speed, two distinct pulleys with different groove numbers (12 and 24) are fixed on the shaft end of the motor and drive two sets of cylinders each. Cylinders 1 and 2 constitute a set and synchronize the motion. Their rotation speed is the same as or twice that of cylinders 3 and 4.

There are three modes of gust excitation considered in this experiment: sine dwell with a single frequency, periodic angle of attack with two harmonic frequency components, and linear frequency sweep. They are controlled by a Macintosh II-Ci personal computer. The control program is included so that the experimentalist can stop the frequency sweep and dwell at any frequency during the test run.

Two gust generator configurations called configuration A and configuration B were used. Configuration A has only two vanes and uses cylinders 1 and 4. The distance between these vanes is 12 in., as shown in Fig. 1. Configuration B has a smaller distance between the two vanes, i.e., 4 in., and uses cylinders 2 and 3.

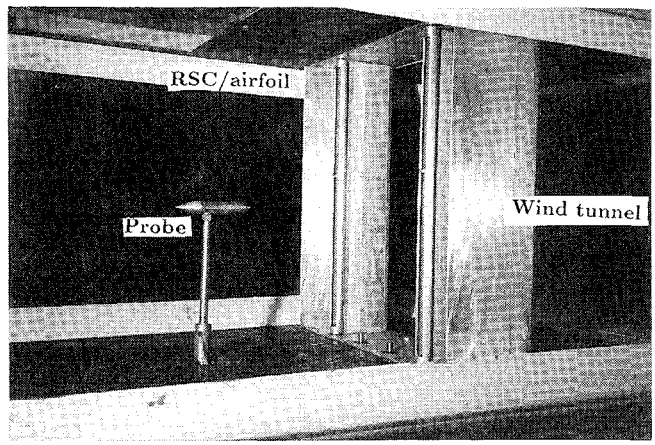

Fig. 1 Photograph of experimental apparatus.

III. Simplified Aerodynamic Theory

To obtain a design estimate of the gust generation capabilities of the proposed system an analysis was made of a simple conceptual mathematical model of a two-airfoil gust generator system (Fig. 2a). This analysis follows that of Reed.[10] For simplicity, the flowfield is assumed to be quasisteady, i.e., k is small and wind-tunnel wall effects are neglected. The problem is to determine the magnitude of the gust velocities induced at a point in this gust flowfield. Take the coordinates of the space point p in the XYZ coordinate system as x_p, y_p, and z_p as shown in Fig. 2a. The lift generated by each RSC/airfoil is approximately represented by a linear segment vortex of strength Γ located at the quarter chord of the RSC/airfoil system. The Biot–Savart law is used to determine the gust flowfield induced by these linear segment vortices. In vector notation, the elementary velocity $d\boldsymbol{v}$ induced at the point p by an element $d\boldsymbol{s}$ belonging to Γ is expressed as follows:

$$d\boldsymbol{v} = \frac{\Gamma}{4\pi}\frac{d\boldsymbol{s} \times \boldsymbol{l}}{l^3}$$

The total induced velocity $\boldsymbol{v}$ at that point becomes

$$\boldsymbol{v} = \frac{\Gamma}{4\pi}\int_c \frac{d\boldsymbol{s} \times \boldsymbol{l}}{l^3}$$

As shown in Fig. 2a, the plane velocity vector v_2 induced by Γ_2 can be represented by

$$v_2 = \Gamma_2/2\pi R_2$$

where

$$R_2 = \sqrt{x_p^2 + (y_0 - y_p)^2}$$

Similar to the previous derivation, the velocity vector $\boldsymbol{v}_1$ at the same point p induced by Γ_1 can also be obtained. The resultant lateral Δw and longitudinal Δu gust velocities induced at that point by each of the two vortices are

$$\Delta w = v_{1y} + v_{2y} = \frac{x_p}{2\pi}\left(\frac{\Gamma_1}{R_1^2} + \frac{\Gamma_2}{R_2^2}\right) \tag{1}$$

$$\Delta u = v_{1x} + v_{2x} = \frac{1}{2\pi}\left[\frac{\Gamma_1(y_0 + y_p)}{R_1^2} - \frac{\Gamma_2(y_0 - y_p)}{R_2^2}\right] \tag{2}$$

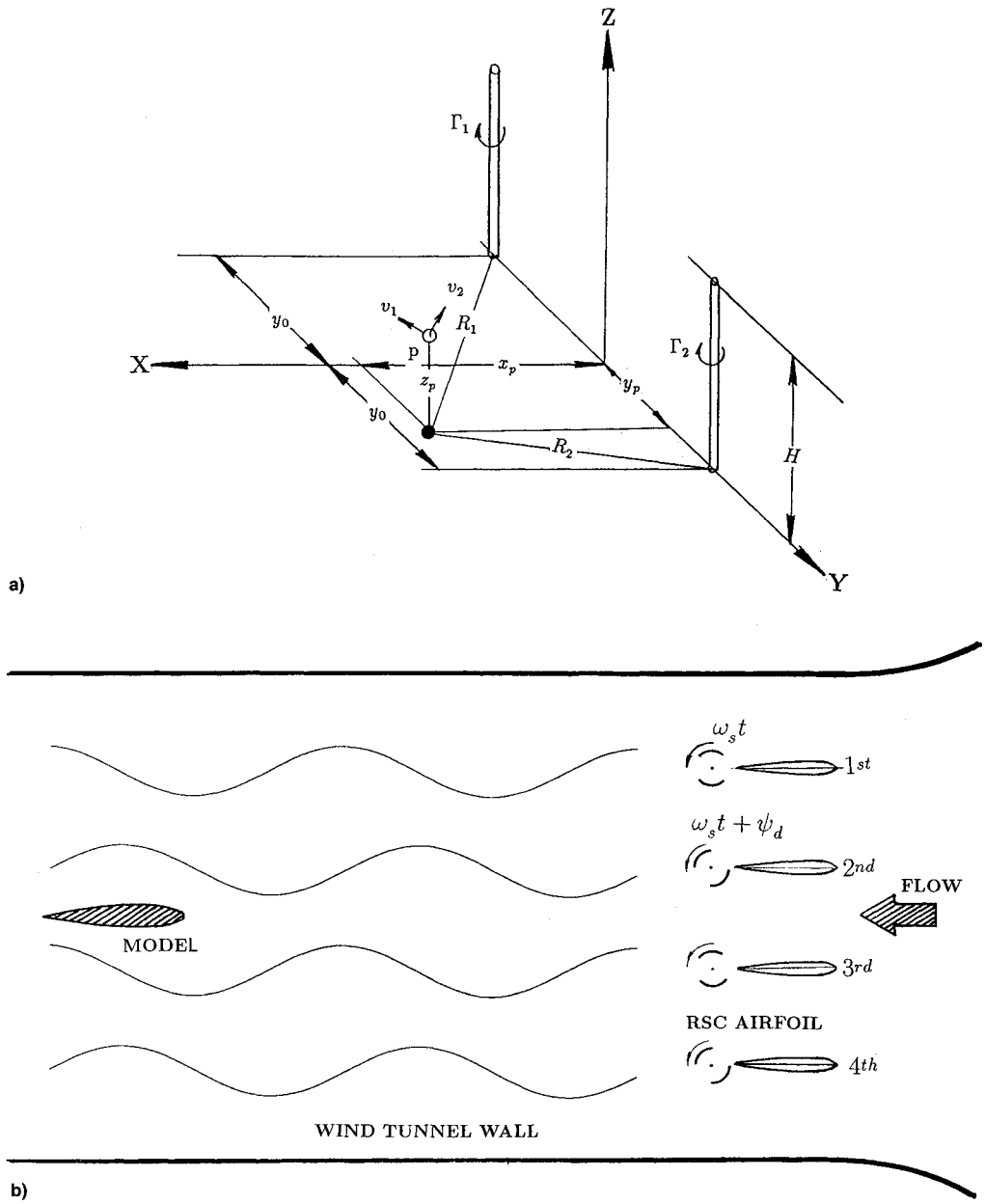

Fig. 2 a) Simple theoretical aerodynamic model and b) sketch of a gust generator with four RSC/airfoil systems.

where

$$R_1 = \sqrt{x_p^2 + (y_0 + y_p)^2}$$

The vortex strength and the lift coefficient for a two-dimensional RSC/airfoil are related by the equation:

$$\Gamma = \tfrac{1}{2} C_{l_{eq}} u(c + d)$$

By matching the wind-tunnel experimental data measured in the present study, an appropriate equivalent lift coefficient for the RSC/airfoil gust generator can be inferred. If there is a phase difference, $\psi_d = \psi_1 - \psi_4$ or $\psi_2 - \psi_3$ between two cylinders (ψ_1, ψ_2 ... are the initial phase angle of the cylinders), then the lift coefficients for the two distinct airfoils in the cascade can be represented approximately as follows:

$$\begin{aligned} C_{l1} &= C_{l_{eq}} C(k) \sin 2\omega_s t \\ C_{l2} &= C_{l_{eq}} C(k) \sin 2(n\omega_s t + \psi_d) \end{aligned} \tag{3}$$

where n denotes the rotational speed ratio of cylinder 1 or 2 to cylinder 4 or 3. The use of $C(k)$ to modify the steady flow relations is consistent with our quasisteady assumption made earlier.

The gust angle of attack and longitudinal gust velocity are given by

$$\alpha_g = \Delta w/u = \frac{C_{l_{eq}} C(k) \bar{x}_p}{4\pi} \left[\frac{1}{\bar{R}_1^2} \sin 2\omega_s t + \frac{1}{\bar{R}_2^2} \sin 2(n\omega_s t + \psi_d) \right] \tag{4}$$

$$\frac{\Delta u}{u} = \frac{C_{l_{eq}} C(k)}{4\pi} \left[\frac{(\bar{y}_0 + \bar{y}_p)}{\bar{R}_1^2} \sin 2\omega_s t - \frac{(\bar{y}_0 - \bar{y}_p)}{\bar{R}_2^2} \sin 2(n\omega_s t + \psi_d) \right] \tag{5}$$

where the superscript bar denotes distance in chord units and $2\omega_s$ and $2n\omega_s$ are the gust frequencies.

When $y_p = 0$ and $n = 1$, i.e., p is located on the centerline of the wind-tunnel test section and there is a single rotating speed for several cylinders, we have

$$\Delta u/u = 0$$

$$\alpha_g = \frac{C_{leq}C(k)}{4\pi}\frac{\bar{x}_p}{\bar{R}_1^2}[\sin 2\omega_s t + \sin 2(\omega_s t + \psi_d)]$$

The magnitude of gust intensity can be varied by changing the phase difference ψ_d. When two cylinders rotate in phase ($\psi_d = 0$ deg), the lateral gust intensity is a maximum and the longitudinal intensity is zero; when $\psi_d = 90$ deg and the cylinders are out of phase, the net induced lateral gust velocity is zero and the longitudinal velocity is a maximum.

A lateral gust attenuation factor A can be defined by the following ratio for $y_p = 0$:

$$A = |\alpha_g|/|\alpha_g|_{\psi=0}$$

It is

$$A = \tfrac{1}{2}\sqrt{(1 + \cos 2\psi_d)^2 + \sin^2 2\psi_d}$$

A sketch of a gust generator with four RSC/airfoil systems and a gust flowfield pattern is shown in Fig. 2b.

IV. Experimental Measurements

Experimental measurements included the equivalent lift coefficient for an RSC/airfoil and the gust flowfield generated by a gust generator in the wind tunnel. The measurements were performed in the Duke University low-speed wind tunnel. The wind tunnel is a closed-circuit tunnel with a test section of 2.3 $\times$ 1.75 ft^2 and a length of 5 ft. The maximum airspeed attainable is 293 ft/s. The stagnation temperature of the airstream is held constant over the range 60–100°F by means of an external air exchange system and tunnel stagnation pressure equals atmospheric pressure at the low Reynolds number operating conditions.

A. Static Equivalent Lift Coefficient for an RSC/Airfoil

The RSC/airfoil system used for the static equivalent lift coefficient measurement is three times larger than that of the gust generator configuration. This is for convenience in measuring the static aerodynamic pressure distribution. The airfoil is set at zero angle of attack. The RSC is statically rotated from 0 to 180 deg and then the pressure distribution on the airfoil surface and the lift force of the RSC are measured. The static equivalent lift coefficient for an RSC/airfoil is determined using an integral of the pressure distribution on the airfoil and a direct lift measurement of RSC. It is defined as

$$C_{leq} = \frac{2(dL_a + dL_{rsc})}{\rho u^2(c + d)}$$

The experimental model and measurement technique are described next.

A two-dimensional NACA 0012 airfoil model measuring 12 in. in chord and 21 in. in span was mounted vertically across the test section from the tunnel floor. A gap of approximately one-sixteenth in. existed between the ends of the model and the wind-tunnel walls. There are 35 orifices 0.046 in. in diameter used for pressure taps that are symmetrically distributed over the upper and lower surfaces of the midspan, respectively. These orifices are connected to a scanivalve system, a standard static pressure measurement system in the wind tunnel.

The RSC is made by using a special manufacturing technique. The cylinder itself is made from a special tube with an o.d. of 3 in. and a thickness of three-eighths inch. The slot is symmetrical with a 45-deg center angle. A top plate with a thickness of one-fourth inch is mounted on the top end of the RSC and a root bracket fixed on the bottom end of the RSC that is connected to a rotating support of a wind-tunnel balance. The RSC is mounted vertically and cantilevered from the rotating support behind the airfoil. The gap between the top of RSC and the ceiling of tunnel is one-sixteenth inch. The gap between the o.d. of the RSC and the trailing edge of airfoil can be adjusted by moving the airfoil root support. A photograph of the RSC/airfoil model in the wind tunnel is shown in Fig. 3.

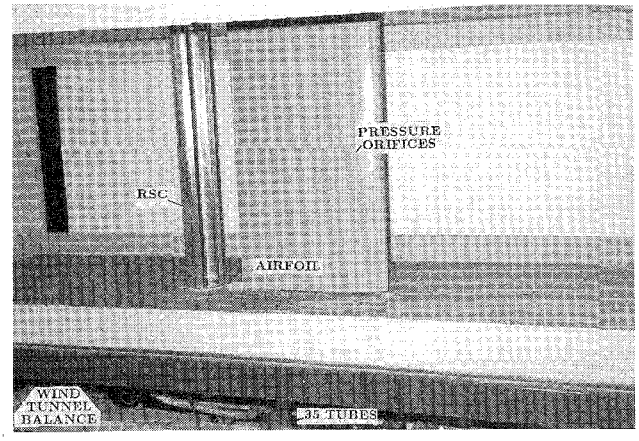

Fig. 3 Photograph of RSC/airfoil model for measuring lift coefficient.

The output of the measured static pressure through the scanivalve system was directly recorded on a Macintosh IIci computer through a data acquisition package, NB-MIO-16 board and an analysis software, LabVIEW 2. The wind-tunnel balance with a readout instrument was used to measure directly the lift force of the RSC system. A rotating controller was used to control the rotational angles of the RSC from 0 to 180 deg.

B. Gust Flowfield

The velocities Δu and Δw (or hence, α_g, which is equal to $\Delta w/u$), were measured with a differential pressure probe mounted on a bar that is located at a certain position in the gust flowfield. The bar was attached to a stand fixed on a support table that can be adjusted to any longitudinal position along the tunnel centerline (called the X axis), to any lateral position along the tunnel spanwise direction (called the Y axis) at $X = 7$ in., and also to any position along the vertical direction of the tunnel (called the Z axis) at $Y = 0$.

The pressure probe consisted of two tubes or claws, oriented at 90 deg to one another in the horizontal plane for measuring the lateral gust and a pitot tube located at the center of the probe for measuring the longitudinal gust. The ends of the tubes protrude from a slender aerodynamic housing, which is oriented in the wind tunnel such that the angle between the tubes is bisected by the freestream. The tubes are connected to two ± 0.1804-psi differential pressure transducers with a high-level voltage output, which is located outside of the wind tunnel and measures the pressure difference in the lateral and longitudinal directions, respectively. The configuration of this probe is similar to a yaw meter of the five-hole probe. For the principle of the gust flowfield measurement, see Ref. 12. A gust of magnitude Δw creates an effective angle of attack, $\tan \alpha_g = \Delta w/u$, relative to the centerline. A photograph of the measurement apparatus is shown in Fig. 1.

V. Experimental Results and Discussion

A. Static Equivalent Lift Coefficient and Correlation with Theory

A typical experimental and theoretical static lifts per span length of the airfoil surface dL_a and the RSC dL_{rsc} vs rotational angles of RSC for the gap value $\bar{e} = 0.08$ and airflow velocity

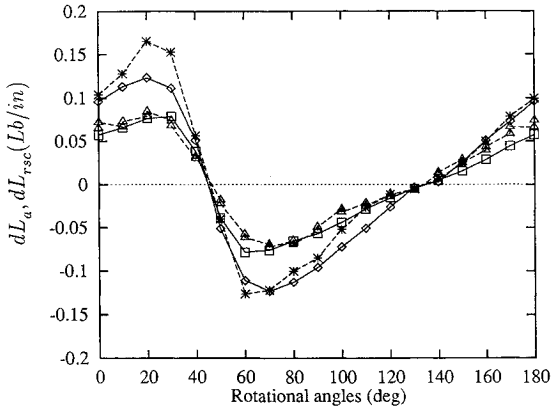

Fig. 4 Theoretical and experimental static lifts per span length of airfoil and RSC vs rotational angles of RSC for $\bar{e}$ = 0.08 and u = 20 m/s. The symbols ◇ and □ are for the theoretical airfoil and RSC forces and * and △ are for the experimental airfoil and RSC forces.

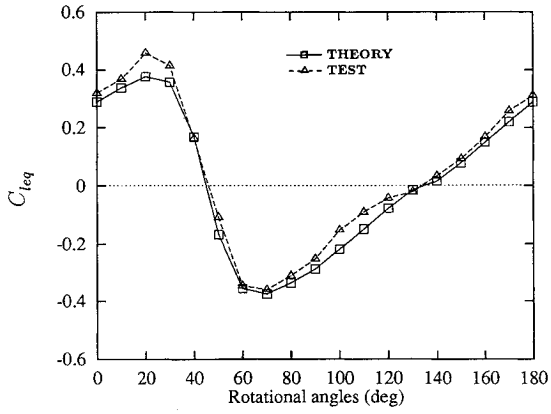

Fig. 5 Theoretical and experimental static equivalent lift coefficients of RSC/airfoil vs rotational angles of RSC for $\bar{e}$ = 0.08 and u = 20 m/s.

u = 20 m/s, is shown in Fig. 4. In this figure, the symbols ◇ and □ are for the theoretical airfoil and RSC forces, and * and △ for the experimental airfoil and RSC forces. Only a half cycle of RSC rotation (from 0 to 180 deg) is needed due to the symmetry of the RSC. The periodic response in rotation angle can be approximately represented as a dominant sinusoidal wave with a periodic phase angle of a one-half cycle of RSC rotation and a higher harmonic component with a periodic phase angle of one-fourth cycle of RSC rotation. The theoretical and experimental results are close except for some points near the rotational angle, 20 deg. In this narrow range, the pressure distribution on the airfoil surface is specially sensitive to the RSC motion. Corresponding to Fig. 4, the theoretical and experimental equivalent lift coefficients C_{leq} vs rotational angles of RSC is shown in Fig. 5. From the fast Fourier transform (FFT) analysis of these data, the theoretical and experimental equivalent lift coefficient are 0.31 and 0.39, respectively, for the dominant periodic component. The maximum lift response is located at ψ_s = 20 deg and the minimum lift response is located at ψ_s = 70 deg. At ψ_s = 45 deg and ψ_s = 135 deg the lift responses are zero. These results are physically plausible due to the RSC symmetry at a zero lift position. The agreement between theory and experiment is good. The theoretical numerical simulation uses FIDAP. The flow is assumed to be quasisteady, turbulent, incompressible and two dimensional (for details see Ref. 13).

Figure 6 shows the variation of the numerically simulated and experimental static lift coefficient of the airfoil (relative to c) with the RSC rotational angles, for several gap values. The gap values are $\bar{e}$ = 0.03, 0.08, and 0.30, and the airflow velocity u = 20 m/s. The purpose of this test is to observe the variation of the airfoil lift coefficient induced by rotating the RSC and the effects of the RSC position. It is found that the lift coefficient decreases as the gap value increases. It is believed that the lift coefficient should be zero when the gap value is large enough. Also note that the differences between the experimental and the numerically simulated lift coefficients increase as the gap decreases.

B. Gust Flowfield

The gust flowfield experiments included four typical cases. They are a single constant rotating speed for all cylinders, two different cylinder rotating speeds, a continuous linear frequency sweep gust, and a specific gust flowfield.

1. Single Constant Rotating Speed for all Cylinders

In this section, we discuss gust flowfield characteristics for a constant single rotating cylinder speed for configuration A.

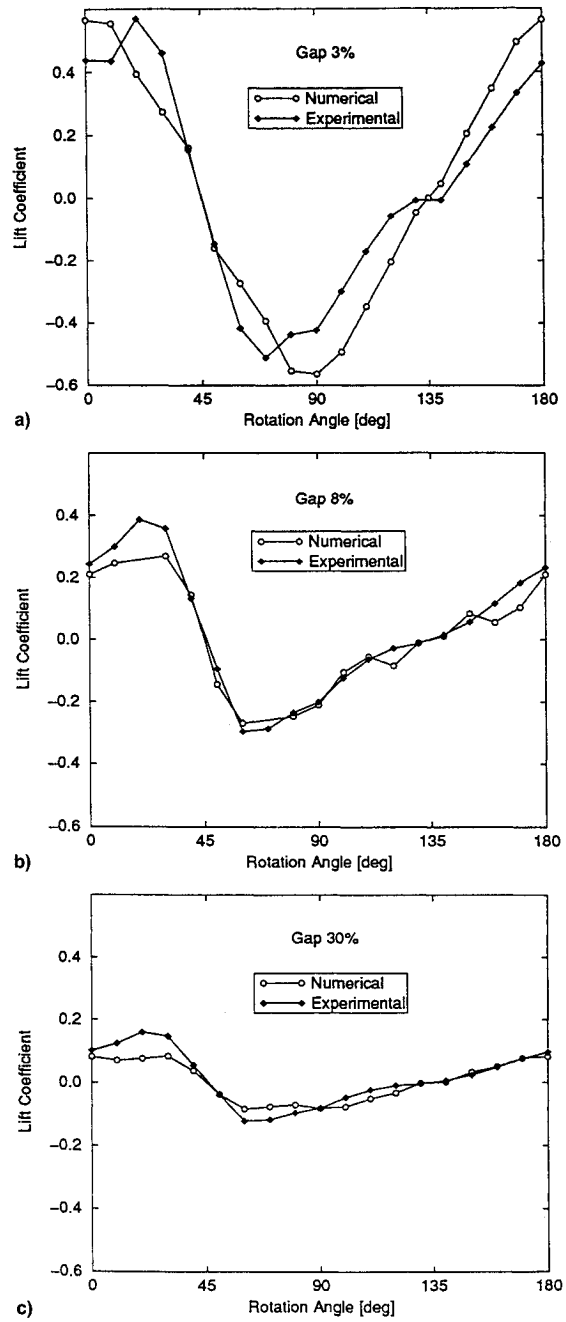

Fig. 6 Theoretical and experimental airfoil lift coefficient vs rotational angles of RSC for u = 20 m/s and several gap values, for $\bar{e}$ = a) 0.03, b) 0.08, and c) 0.3.

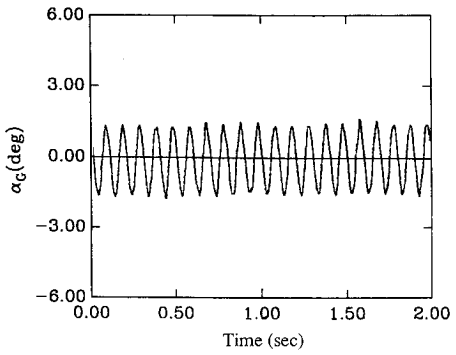

Fig. 7 Measured gust angle wave for ω_s = 5 Hz, $\bar{L}$ = 1, and u = 25 m/s for configuration A.

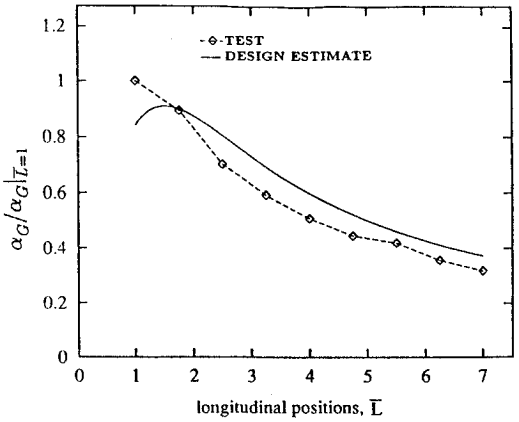

Fig. 8 Relative gust angle vs the longitudinal coordinate for ω_s = 5 Hz and u = 25 m/s.

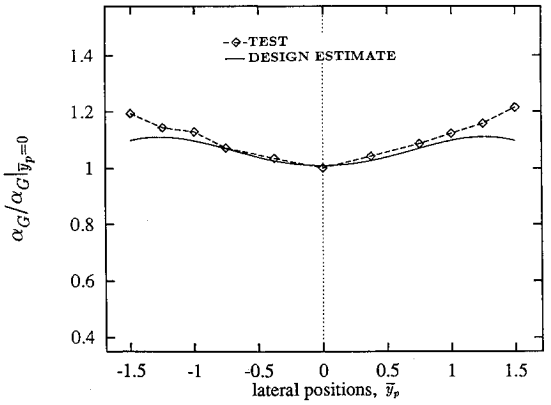

Fig. 9 Relative gust angle vs the lateral coordinate for $\bar{L}$ = 1.75.

A typical measured lateral gust wave generated by the RSC gust generator is shown in Fig. 7. The pressure probes are placed at L = 4 in. from the cylinder center in the horizontal direction, y_p = 0 in. in the lateral direction, and H = 10.5 in. from the bottom of the tunnel in the vertical direction. The results from the experiment indicate that there is a $4\omega_s$ frequency component in addition to a dominant frequency component, $\omega_1 = 2\omega_s$, but this component is not very significant. A relatively pure lateral sinusoidal gust wave is obtained. Results from the theoretical study indicate that α_g is a sine function with $2\omega_s$, as shown in Eq. (4). The difference between the theory and experiment comes from the nature of the approximate aerodynamic theory. The theory does not take into account the interaction between the wakes behind the two rotating cylinders. For the present configuration A an expected better agreement between the simplified theory and the experimental results is obtained. Next, we will discuss the lateral gust flowfield characteristics and the effects of the basic parameters of the RSC gust generator on the gust intensity only for configuration A. On basic theoretical grounds, one anticipates that these experimental results may be collapsed to nearly universal curves independent of the equivalent lift coefficient of RSC/airfoil. The experimental results are nondimensionalized by a given gust angle in the flowfield and are displayed in Figs. 8–12. The gust angles are indicated by $\alpha_G|_{\bar{L}=1}$, $\alpha_G|_{\bar{y}_p=0}$, $\alpha_G|_{\bar{H}=0.5}$, $\alpha_G|_{k=0}$, and $\alpha_G|_{\psi_d=0}$ corresponding to $\bar{L}$ = 1, $\bar{y}_p$ = 0, $\bar{H}$ = 0.5, k = 0, and ψ_d = 0.

Figure 8 shows the variation of the relative gust angle $\alpha_G/\alpha_G|_{\bar{L}=1}$ vs the longitudinal coordinate $\bar{L}$ for u = 25 m/s, ψ_d = 0

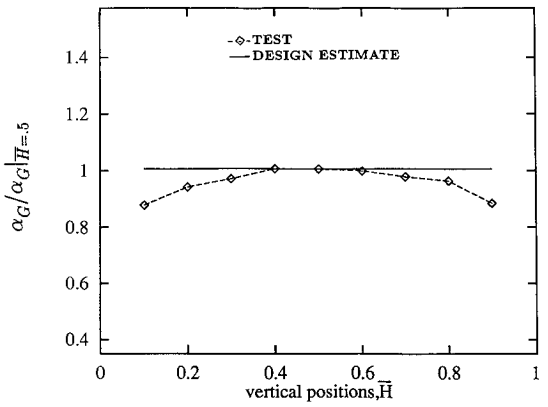

Fig. 10 Relative gust angle vs the vertical coordinate for $\bar{L}$ = 1.75.

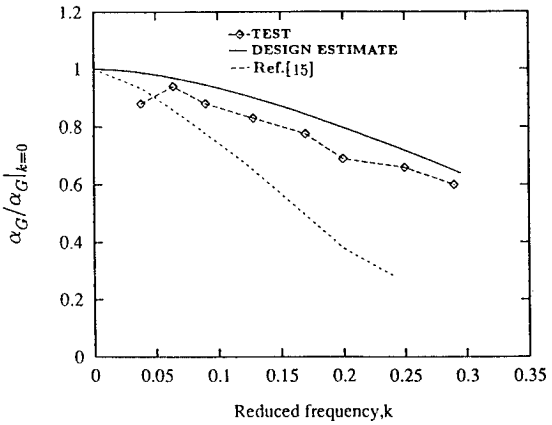

Fig. 11 Relative gust angle vs reduced frequency k for $\bar{L}$ = 1.75.

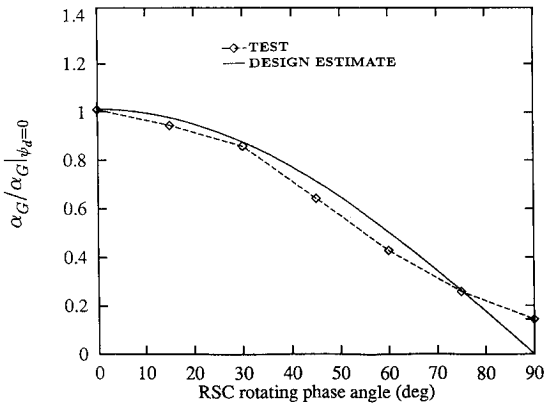

Fig. 12 Relative gust angle vs the dynamic phase difference for $\bar{L}$ = 1.75 and $\bar{y}_p$ = 0.

deg, and ω_s = 5 Hz. As $\bar{L}$ increases, the gust angle decreases. A comparison of simplified theoretical and experimental results is also shown in Fig. 8. The results show good agreement.

Figure 9 shows the relative gust angle $\alpha_G/\alpha_G|_{\bar{y}_p=0}$, vs the lateral coordinate of the tunnel for ψ_d = 0 deg, $\bar{L}$ = 1.75, u = 25 m/s, and ω_s = 5 Hz. The gust velocities have a small variation with the lateral position and the variation is symmetrical relative to the tunnel centerline. A comparison of theoretical and experimental results is also shown in Fig. 9. The agreement for the gust angle is good in the range near the tunnel center. A larger difference between the theory and experiment occurs at $\bar{y}_p = \mp 1.5$. This is because the experimental effect of wake interaction behind the cylinders is stronger at $\bar{y}_p = \mp 1.5$.

Figure 10 shows the variation of the maximum relative gust angle $\alpha_G/\alpha_G|_{\bar{H}=0.5}$ with the vertical coordinate in the symmetrical plane of the tunnel for $\bar{L}$ = 1.75, u = 25 m/s, and ω_s = 5 Hz. $\bar{H} = H/H_w$ = 0.5 is the centerline of the tunnel. It is found that the gust flow variation along the vertical axis is symmetrical relative to the centerline. The quantitative agreement between the present two-dimensional theory and experimental data is fair. Near the tunnel top and bottom the theoretical values are larger than the experimental values. This is because the end parts of the RSC have a three-quarter-in. length with no slotted cylinder for mounting the bearings. Other differences may come from the effects of the tunnel wall and three-dimensional aerodynamic effects.

In Figs. 9 and 10, the fact that the gust velocity field is relatively uniform in the plane of symmetry and across the test is especially important in such applications as for the test of model helicopter rotors, bridges, or other long slender structures, as shown in Ref. 14.

Figure 11 shows the measured relative gust angle $\alpha_G/\alpha_G|_{k=0}$ vs reduced frequency from k = 0.02 to 0.31, or for a corresponding cylinder rotational speed from ω_s = 1.5 to 12.25 Hz for $\bar{L}$ = 1.75, $\bar{y}_p$ = 0, and u = 25 m/s. As compared with the results from Ref. 15, in which the gust is generated by oscillating biplane vanes mounted on the side wall of the test section entrance, here the gust angle decays with k for $0.01 \leq k \leq 0.24$. For a similar gust field, the results of Ref. 15 show reasonable qualitative agreement with the present one in the range of $0.01 \leq k \leq 0.14$. Theoretical curves from the present model are also plotted in the same figure for comparison. The results of the present theoretical model show fair agreement with experiment.

Figure 12 shows the relative gust angle $\alpha_G/\alpha_G|_{\psi_d=0}$ vs ψ_d for $\bar{L}$ = 1.75, $\bar{y}_p$ = 0, and u = 25 m/s. The rotation of the first cylinder relative to the fourth cylinder is varied from in phase to 90-deg out of phase. The gust intensity decreases as ψ_d increases from 0 to 90 deg. The agreement for gust angle between theory and experiment is reasonably good. Two typical photographs of the gust pattern using the grid-tuft method in the wind tunnel are shown in Fig. 13a for in phase ψ_d = 0 deg and Fig. 13b for out of phase ψ_d = 90 deg cylinder rotation phase angle, respectively. These photographs are consistent with the measured results shown in Fig. 12 in which for ψ_d = 0 deg, the gust amplitude is a maximum at y_p = 0 due to in phase addition and for ψ_d = 90 deg the gust amplitude is much smaller (the lateral gust velocity is theoretically zero at midpoint) due to out of phase cancellation. These results provide additional insight for understanding this gust excitation wave.

Figure 14 shows the effect of varying the section profile of the RSC on the gust strength for ω_s = 5 Hz, $\bar{L}$ = 1.5, $\bar{y}$ = 0, u = 25 m/s, and configuration A. In addition to the base section profile (called model A), five other section profiles of the RSC (called models B–F) were evaluated in the wind-tunnel test. Model B is made from a brass tube with an o.d. of 1 in. and a thickness one-thirty-second in. The slot is symmetrical with a 45-deg center angle. The slot is divided into three spanwise segments, supported by two circular plates with a diameter of 1 in. and a width of one-sixteenth in. Model C is identical with model B except for the 51-deg center angle. Based on the

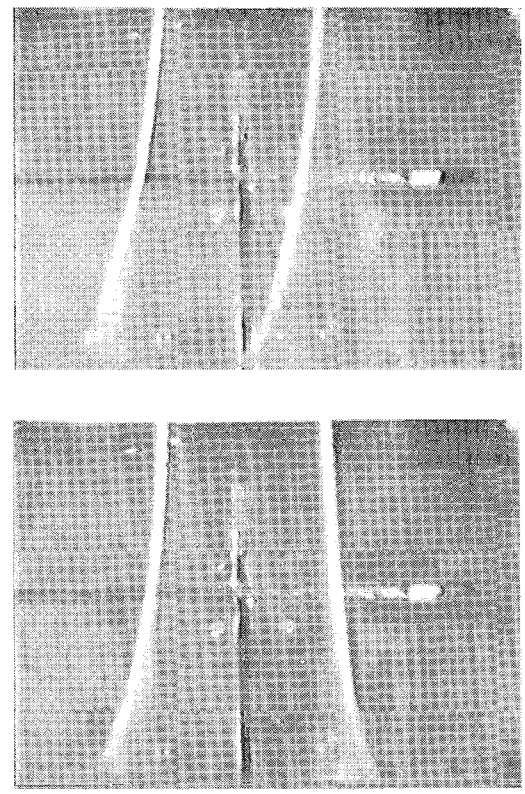

Fig. 13 Measured visual gust wave at $\bar{y}_p = -0.5$ and 0.5: a) in phase ψ_d = 0 and b) out of phase ψ_d = 90 deg.

model B configuration, model D is made in a single crescent section profile instead of the quarter tube section and model E has two crescent section profiles. Model F is similar to model A except for the 27.5-deg center angle as shown in Fig. 12. Compared to the previous results for the base section profile (model A), models B and C produce a larger lateral gust response. The dominant gust angle α_{G1} ($2\omega_s$ frequency component) increases about 16% for model B and 12% for model C. However, the $4\omega_s$ frequency component α_{G2} correspondingly increases by about 100 and 50%, respectively. Model F gives the worst results in that the fundamental lateral gust component decreases and the higher harmonic gust components increase. Models D and E also do not bring the expected improvement for rejection of the higher harmonic gust components. From this figure, the authors conclude that there is an optimum section profile for the RSC to obtain a high performance gust generator. Of those studied here, models A, B, and C have the most promise.

2. Two Different Cylinder Rotating Speeds

In this section, we discuss gust flowfield characteristics for the case of two different cylinder speeds. It is assumed the first cylinder rotating speed is twice as large as that of the fourth cylinder.

A typical measured time history of a gust angle and the corresponding FFT are shown in Figs. 15a and 15b for an airstream velocity u = 15.6 m/s, and cylinder rotation speed, ω_s = 3 and 6 Hz. The pressure probes are placed at $\bar{L}$ = 1, $\bar{y}_p$ = 0, and $\bar{H}$ = 0.5. There are more than two frequency components in the gust wave. The dominant frequencies are $\omega_1 = 2\omega_s$ and $\omega_2 = 4\omega_s$. The other higher harmonic components are smaller.

Two typical examples of the gust flowfield characteristic are shown in Figs. 16 and 17. Figure 16 shows the variation of the relative gust angle divided by gust angle at $\bar{y}_p$ = 0 with the lateral coordinate of the tunnel for $\bar{L}$ = 1.75. There is an asymmetrical variation of the gust velocity distribution relative to the centerline, as expected. The magnitude of frequency com-

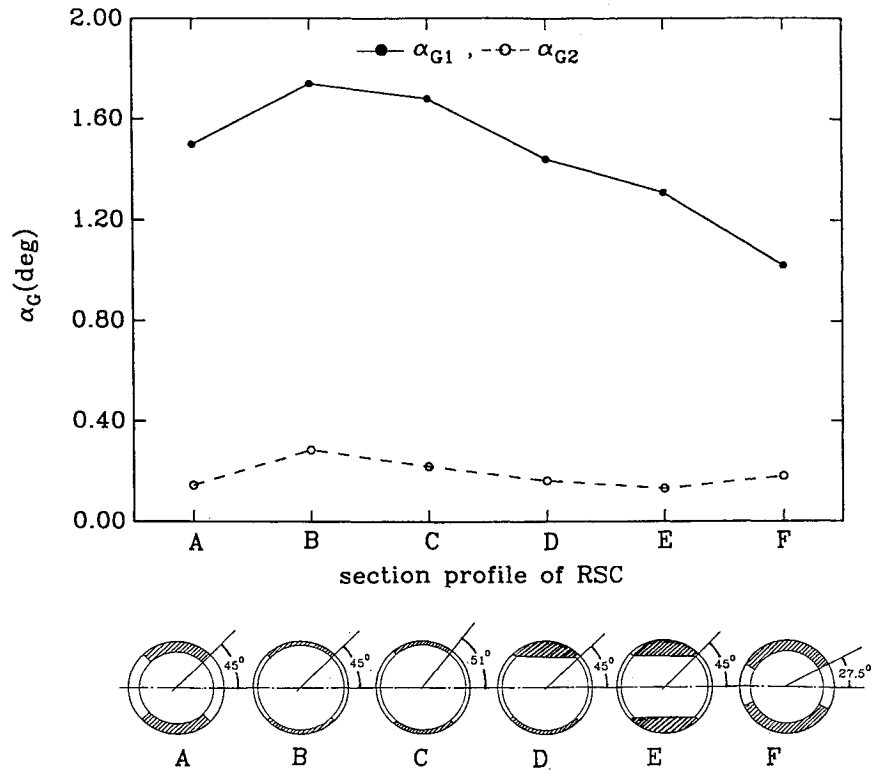

Fig. 14 Gust angle vs section profiles of RSC for $\bar{y}_p = 0$ and $\bar{L} = 1.5$.

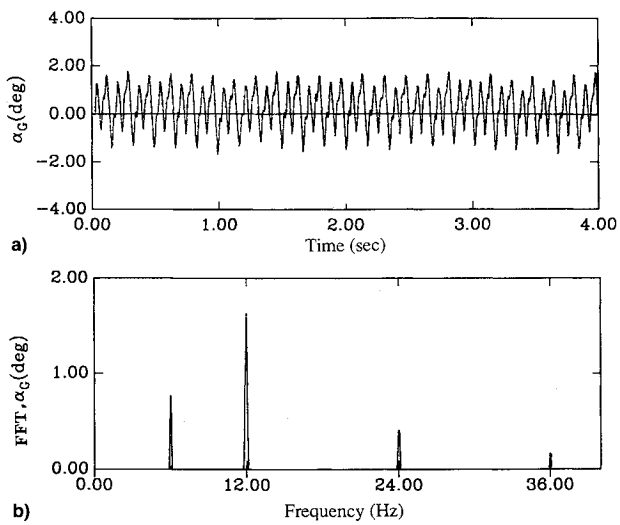

Fig. 15 Measured gust angle for two different cylinder rotating speeds for $\omega_{s1} = 3$ Hz, $\omega_{s2} = 6$ Hz, and $u = 15.6$ m/s: for a) time history and b) FFT.

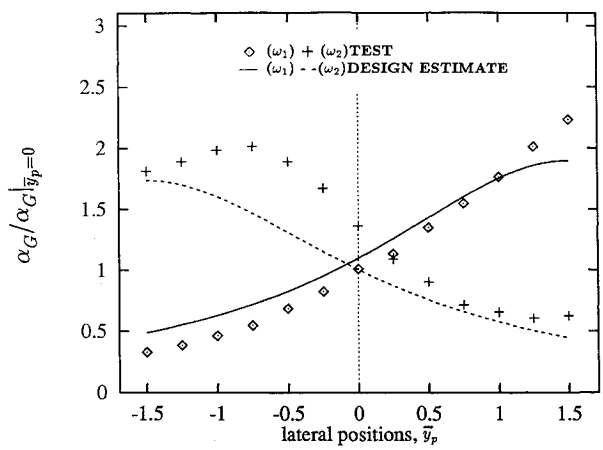

Fig. 16 Relative gust angle vs the lateral coordinate for $\omega_{s1} = 5$ Hz, $\omega_{s2} = 10$ Hz, $\bar{L} = 1.75$, and $u = 25$ m/s.

ponent depends significantly upon the lateral position. Near the first cylinder the gust velocity is dominated by $\omega_2 = 4\omega_s$, and near the fourth cylinder by $\omega_1 = 2\omega_s$. The theoretical results are also plotted in this figure. The qualitative agreement for the ω_1 frequency component is better than that for the ω_2 frequency component. This is because the higher harmonic component $2\omega_1$ induced by the fourth cylinder is added to the ω_2 frequency component. The composite ω_2 components are larger than the theoretical prediction.

Figure 17 shows the relative gust angle divided by the gust angle at $k = 0$ vs reduced frequency, from $k = 0.02 - 0.31$ for $\bar{L} = 1.75$ and $\bar{y}_p = 0$. The gust angle decays with increasing k for the ω_1 components, but for the ω_2 components there is a peak at $k = 0.128$. An aerodynamic theory to explain this response of the gust field at these frequencies has not yet been developed. A probable reason may be that the ω_2 component is a synthesis that includes dominant frequency excitation from rotating cylinder 1 and the induced higher frequency component produced by cylinder 4 in the range of $k = 0.128$. The theoretical ω_1 and ω_2 results are also plotted in this figure. The ω_1 theoretical results are reasonably close to the measured data.

3. *Continuous Linear Frequency Sweep Gust*

LabVIEW 2 software is also used to create a continuous ramp voltage vs time and to obtain a continuous linear frequency sweep speed for cylinders first and fourth of configuration A. The ramp rate and period of this output voltage are controlled by the computer.

Figure 18a shows a typical measured lateral gust wave generated by the linear frequency sweep for an airstream velocity of $u = 10$ m/s, and cylinder rotational speeds from 0 to 20 Hz in 4 s in the case of configuration A. A corresponding power spectral density (PSD) plot is shown in Fig. 18b. A relatively random lateral gust wave with a narrow frequency band PSD

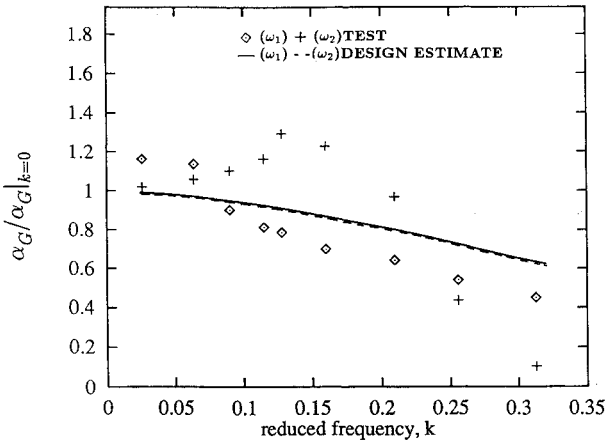

Fig. 17 Relative gust angle vs reduced frequency k for ω_{s1} = 5 Hz, ω_{s2} = 10 Hz, $\bar{L}$ = 1.75, and u = 25 m/s.

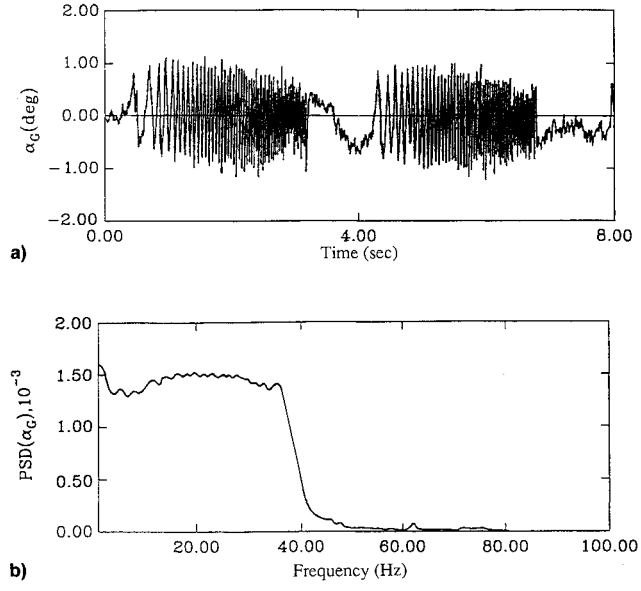

Fig. 18 Experimental lateral gust of linear frequency sweep for ω_s = 0–20 Hz, u = 10 m/s, and sweep duration 4 s: for a) time history and b) PSD.

is obtained. It is noted that the experimental result has a 0.68-s time delay Δt as shown in Fig. 18a. This is because of the rotational inertia of the dc motor.

The PSD measurement data use an averaging procedure over 200 sweep periods. The effect of random tunnel turbulence generally can be neglected for these experiments.

For Cases 1–3, a typical application is described in Ref. 16 for the gust response of a flexible rotor blade.

4. Specific Gust Flowfield

To simulate the aerodynamic environment of aeroelastic problems with either random or nonrandom parametric excitation, the present gust generator system can be used to generate a specific gust excitation flowfield. A typical application is discussed in Ref. 17 for simulating the aerodynamic environment of a rotating rotor blade in forward flight. The RSC gust generator can be used to produce a single harmonic gust wave and also turbulence with uniform power spectral density over a certain frequency band in the lateral and longitudinal directions. The second and third cylinders are used to generate the sinusoidal longitudinal gust, while the first and fourth cylinders are used to generate a lateral frequency sweep gust. The two pairs of gust generators are controlled by an execution software written in the LabVIEW.

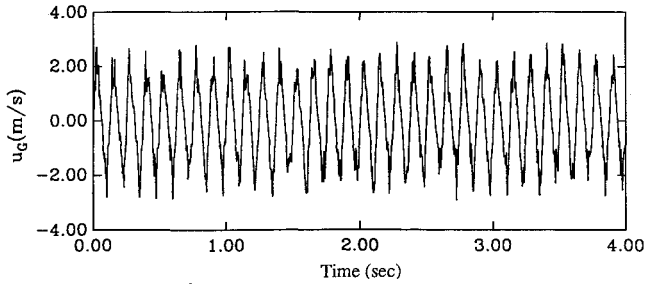

Fig. 19 Measured time history of the longitudinal gust generated by configuration B for ω_s = 4 Hz, y_p = 0, and u = 23 m/s.

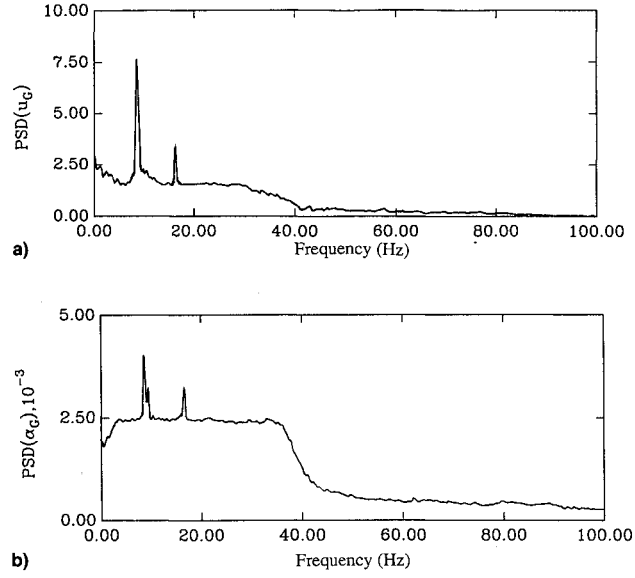

Fig. 20 Measured gust PSD for y_p = 2 in. and u = 23 m/s: for a) longitudinal and b) lateral gusts.

The gust flowfield behavior depends upon the lateral position y_p. At y_p = 0, i.e., the tunnel centerline position, a nonrandom parametric excitation flowfield is obtained. A typical measured time history of longitudinal gust for configuration B is shown in Fig. 19. The airstream velocity and cylinder rotation speed are u = 23 m/s and ω_s = 4 Hz, respectively. The pressure probes are placed at L = 6 in. and H = 10.5 in. From corresponding PSD analysis, it is found that the dominant signal is a single sine wave with a detectable second harmonic component. Background noise due to the shed vortices behind the rotating cylinders is also present, but is not very strong. The power spectra from measured lateral gust wave generated by the linear frequency sweep of RCS first and fourth for an airstream velocity of u = 23 m/s, and cylinder rotation speeds from 0 to 20 Hz in 2.8 s is similar to Fig. 18. A relatively uniform power spectral density in the 0–40-Hz frequency band is obtained. Also, small first and second harmonic components arising from the second and third cylinders are present in the lateral gust.

At the y_p = 2-in. position, a random parametric excitation flowfield is obtained. The measured gust PSD plots are shown in Figs. 20a and 20b. Figure 20a is for the longitudinal gust and Fig. 20b is for the lateral gust. Note that when $y_p \neq 0$, each rotating cylinder can produce both longitudinal and lateral gusts, but the quantitative contribution is different. Comparing Figs. 20a and 20b to the PSD plot of Fig. 19, we find that for the longitudinal signal, the gust component of the continual frequency sweep excitation generated by the first and fourth cylinders is added to the longitudinal gust. The second harmonic frequency component (16 Hz) and the background white noise slightly increase, and the dominant frequency component (8 Hz) slightly decreases. For the lateral signal, the 8-

and 16-Hz frequency components generated by the second and third cylinders are added to the lateral gust. The variations of the background noise and frequency sweep gust components are small.

VI. Concluding Remarks

1) Compared to other successful gust generators, e.g., rotating vanes, the RSC gust generator can produce a controllable single or multiple harmonic lateral gust wave; also, the gust strength can be varied by adjusting the geometrical cylinder parameters; the configuration is simple and the cost is low.

2) In addition to the dominant frequency component in the gust wave, higher harmonic frequency components are also created by the RSC gust generator. It is found that the higher harmonic components depend significantly on the distance between two cylinders, the distance behind the rotating cylinder and the section profile of the RSC.

3) The RSC gust generator can also generate a controllable longitudinal gust wave and a specific random or periodic gust flowfield.

4) An approximate two-dimensional aerodynamic theory to describe the gust wave produced by the present gust generator has been developed. It does give a qualitative and approximate description of the flowfield that is very useful for a design estimate. However, the experimental results do indeed demonstrate that the flowfield in the working section of the wind tunnel is three dimensional. The simplified aerodynamic theory proposed, although useful for design, needs to be further improved.

5) The results of a finite element fluid code show encouraging agreement with experiment for an RSC/airfoil configuration with a fixed rotational angle.

Acknowledgments

This work was supported by the Army Research Office under Grant DAAL03-87-K-0023; Gary Anderson is the Technical Monitor and his encouragement and support are deeply appreciated. The authors have also greatly benefited from discussions with Wilmer H. Reed III.

References

[1]Gilman, J., Jr., and Bennett, R. M., "A Wind Tunnel Technique for Measuring Frequency Response Functions for Gust Load Analyses," *Journal of Aircraft*, Vol. 3, No. 6, 1966, pp. 535–540.

[2]Huston, D. R., and Bosch, H. R., "Active Modeling of Turbulence for Section Model Studies," 16th U.S.–Japan Joint Panel on Wind and Seismic Effects, National Bureau of Standards, Gaithersburg, MD, May 1984.

[3]Huston, D. R., and Bosch, H. R., "The Effects of Large-Scale Upstream Gusting on the Aeroelastic Behavior of Section Models," 18th U.S.–Japan Joint Panel on Wind and Seismic Effects, Gaithersburg, MD, May 1986.

[4]Buell, D. A., "An Experimental Investigation of the Velocity Fluctuations Behind Oscillating Vanes," NASA TN D-5543, Nov. 1969.

[5]Bicknell, J., and Parker, A. G., "A Wind-Tunnel Stream Oscillating Apparatus," *Journal of Aircraft*, Vol. 9, No. 6, 1972, pp. 446, 447.

[6]Parker, A. G., and Bicknell, J., "Some Measurements on Dynamic Stall," *Journal of Aircraft*, Vol. 11, No. 7, 1974, pp. 371–374.

[7]Poisson-Quinton, P., "Note on a New V/STOL Rig in the S1 Modane Sonic Tunnel," Third AGARD Meeting on V/STOL Tunnels, ONERA, Amsterdam, Feb. 1972.

[8]Ham, N. D., Bauer, P. H., and Lawrence, T. L., "Wind Tunnel Generation of Sinusoidal Lateral and Longitudinal Gust by Circulation Control of Twin Parallel Airfoils," NASA CR 137547, Aeroelastic and Structures Research Lab., TR 174-3, Aug. 1974.

[9]Jones, W. P., and Moore, J. A., "Flow in the Wake of a Cascade of Oscillating Airfoil," *AIAA Journal*, Vol. 10, No. 12, 1974, pp. 1600–1605.

[10]Reed, W. H., III, "Conceptual Design of a Wind Tunnel Gust Generator and Rotor Blade Model with Feedback Control," Dynamic Engineering, Inc., Document D-409, Newport News, VA, June 1991.

[11]Reed, W. H., III, Gold, R. R., Kehoe, M. W., Nilsson, B., and Schippers, P., "An Excitation System for Aircraft Flutter Testing: Some Highlights of Flight Test Applications," *Proceedings of the 24th Annual Symposium of the Society of Flight Test Engineers*, Seattle, WA, 1993.

[12]Yates, E. C., Jr., and Fox, A. G., "Steady-State Characteristics of a Differential-Pressure System for Evaluating Angles of Attack and Sideslip of the Ranger IV Vehicle," NASA TN D-1966, Nov. 1963.

[13]Cizmas, P. G. A., Tang, D. M., and Dowell, E. H., "Computation of the Flow About a Rotating Slotted Cylinder in a Wind Tunnel," *Journal of Aircraft* (to be published).

[14]Mirick, P. H., Hamouda, M.-N. H., and Yeager, W. T., Jr., "Wind Tunnel Survey of an Oscillating Flow Field for Application to Model Helicopter Rotor Testing," NASA TM 4224/AVSCOM TR 90-B-007, Dec. 1990.

[15]Abbott, F. T., Jr., "Brief Description on the Characteristics of the Langley Transonic Dynamics Tunnel Airstream Oscillator," NASA TM-82340, Sept. 1968.

[16]Tang, D. M., and Dowell, E. H., "Experimental and Theoretical Study on Nonlinear Response of a Rotor Blade to a Gust," *Applied Mechanics Reviews*, Vol. 47, No. 11, Pt. 2, 1993.

[17]Tang, D. M., and Dowell, E. H., "Response of a Nonrotating Rotor Blade to Lateral Turbulence, Part II: Experiment," *Journal of Aircraft*, Vol. 32, No. 1, 1995, pp. 154–160.